

This is a repository copy of *Comparing Five and Lower-Dimensional Grain Boundary Character and Energy Distributions in Copper : Experiment and Molecular Statics Simulation*.

White Rose Research Online URL for this paper:

<https://eprints.whiterose.ac.uk/183271/>

Version: Accepted Version

Article:

Korolev, Vadim V., Bean, Jonathan J., Nevolin, Yurii M. et al. (3 more authors) (2022) Comparing Five and Lower-Dimensional Grain Boundary Character and Energy Distributions in Copper : Experiment and Molecular Statics Simulation. *Metallurgical and Materials Transactions A: Physical Metallurgy and Materials Science*. pp. 449-459. ISSN 1073-5623

<https://doi.org/10.1007/s11661-021-06500-5>

Reuse

Items deposited in White Rose Research Online are protected by copyright, with all rights reserved unless indicated otherwise. They may be downloaded and/or printed for private study, or other acts as permitted by national copyright laws. The publisher or other rights holders may allow further reproduction and re-use of the full text version. This is indicated by the licence information on the White Rose Research Online record for the item.

Takedown

If you consider content in White Rose Research Online to be in breach of UK law, please notify us by emailing eprints@whiterose.ac.uk including the URL of the record and the reason for the withdrawal request.

1 Comparing five and lower-dimensional grain boundary character and
2 energy distributions in copper: experiment and molecular statics simulation

3 Vadim V. Korolev^a, Jonathan J. Bean^b, Yurii M. Nevolin^c, Yaroslav V. Kucherinenko^d, Keith
4 P. McKenna^e, Pavel V. Protsenko^{a,*}

5 ^aDepartment of Chemistry, Lomonosov Moscow State University, 119991, Leninskoye Gori,
6 1-3, Moscow, Russia

7 ^bDepartment of Material Science and Metallurgy, The University of Cambridge, Cambridge,
8 CB2 3QZ, UK

9 ^cRadiochemistry Department, Frumkin Institute of Physical chemistry and Electrochemistry
10 Russian academy of sciences, 117342, Obruchev street, 40, Moscow, Russia

11 ^dDepartment of Geology, Lomonosov Moscow State University, 119991, Leninskiye Gory,
12 1-1, Moscow, Russia

13 ^eDepartment of Physics, The University of York, York, YO10 5DD, UK

14

15

16

17

18

19

20

21

22

23 *protsenko@colloid.chem.msu.ru

24

25

26 ABSTRACT

27 The misorientation of 515 grain boundaries has been determined using electron back scatter
28 diffraction data from an 18 μm thick copper foil with columnar grain structure and a
29 preferential $\{110\}$ surface orientation. The energy of the grain boundaries was determined
30 from the dihedral angles in the vicinity of grain boundary thermal grooves. The experimental
31 grain boundary energy vs. misorientation angle shows deep minima for the low angle grain
32 boundaries and small minima corresponding to the $\Sigma 3$ and $\Sigma 9$ grain boundaries. Only a small
33 fraction of the coincidence site lattice grain boundaries demonstrate an increased occurrence
34 frequency (compared to a random orientation distribution) and low energy. In parallel, the
35 grain boundary energy for a subset of 400 symmetrical tilt grain boundaries was calculated
36 using molecular statics simulations. There is a good agreement between the experiment and
37 molecular statics modeling.

38 INTRODUCTION

39 The complex network formed by individual grain boundaries (GBs) has a decisive influence
40 on the physicochemical, mechanical, electromagnetic, and other properties of polycrystalline
41 materials^[1]. Understanding the relationship between the crystallographic parameters of GBs
42 and the GB energy has motivated researchers for decades^[2-4]. The continuous development
43 of the microelectromechanical systems (MEMS) industry has accelerated the knowledge on
44 how to process devices, which has resulted in different internal interfaces inside the
45 condensed systems^[1]. The relationships between degrees of freedom (DOF), GBs structures
46 and GBs energies were investigated previously by many researchers^[5-8], but the number of
47 grain boundaries reported in these previous studies are not sufficient to determine the
48 variations of GBs structures and GBs energies in the 5 DOF space. Nevertheless many
49 theoretical models have been proposed to explain this relationship^[5,9-12]. Furthermore, in
50 recent years, it has been established that the GBs are also significantly influenced by
51 microscopic degrees of freedom^[13] and macroscopically identical GBs can differ
52 significantly by the atomic arrangement in the region between adjacent bulk phases^[14].

53 It is important to verify any theoretical approach or computational model using experimental
54 data on both GB geometry and GB energy for a large set of GBs. The most successful
55 approach to determine experimentally the GB energies considers the equilibrium between the
56 three boundary tensions along the triple line. This equilibrium at triple junctions is described
57 quantitatively by the Herring equation:

- 58 ▪ Solid/solid/gas (SSG) capillary equilibrium is established along the line formed by the
59 intersection of the GB plane with the sample surface. The tension of the GB is not
60 balanced by the tensions of free surfaces when the sample surface is flat. Thus, surface
61 deformation occurs and a GB groove is formed. The thermal grooving technique
62 measures the angles in the GB grooves. SSG was previously used for relatively small sets
63 of GBs, most often special GBs with a high degree of symmetry^[15–18]. A key requirement
64 for SSG to yield accurate results is that the material should have an isotropic surface
65 energy.
- 66 ▪ Solid/solid/solid (SSS) capillary equilibrium. When three GBs join along a common triple
67 line in a polycrystal, the dihedral angles between the corresponding GB planes are
68 determined by capillary equilibrium ^[19,20]. This equilibrium is established between three
69 capillary vectors. Each capillary vector is a sum of the GB tension vector (lying in the GB
70 plane orthogonal to the triple line) and a torque term vector (equal in absolute value to the
71 derivative of the GB energy with respect to the angle of rotation of the boundary around
72 the triple line and orthogonal to the GB plane and to the triple line). The capillary vector
73 reconstruction method involves solving a system of equations that describe the local
74 equilibrium in triple junctions (Herring equations) using an iterative procedure. Owing to
75 redundancy in the Herring equations, it is necessary to introduce additional restrictions
76 such as constant GB energy within the local domain of the crystallographic GB
77 parameters.

78 In both SSG and SSS, the objective is to determine the relationship between the GB energy
79 distribution (GBED) and the GB character distribution (GBCD) for all the macroscopic
80 parameters of GBs^[4]. SSG and SSS differ only in how the results are generalized from a
81 finite set of GBs to the five macroscopic degrees of freedom of GBs.

82 In SSG, an extrapolation scheme is used where two important conditions must be met: a
83 reliable set of input data and a suitable functional relationship between the GB energy and
84 crystallographic parameters. The approach proposed by Bulatov^[8], where the results of
85 molecular statics simulations for 388 CSL GBs (periodic length for each grain is no more
86 than $15a_0/2$, where a_0 is the lattice spacing) are used as input data^[6,7], has become widely
87 used for calculation of GB energy for arbitrary misorientation ^[21–23]. However, it was
88 demonstrated by comparing the simulated and experimental data that only the $\Sigma 3$ and $\Sigma 9$
89 GBs agree^[24].

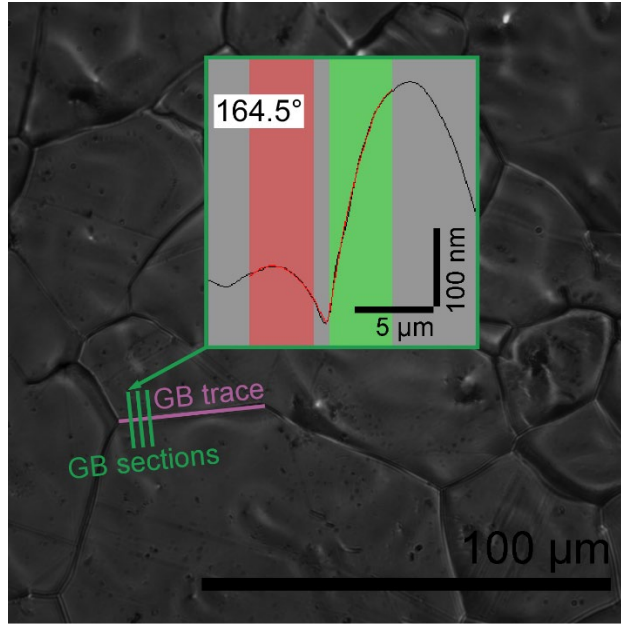
90 In the SSS calculation using the Morawiec method, a discretization of the parameter space
91 where the energy is kept constant within each domain is performed. For highly symmetric
92 GBs where the GBED(GBCD) is pronounced, the assumption that the GB energy is constant
93 should be treated with caution and the results of this method strongly depend on the size of
94 the initial sample (filling density) and the size of the domains. Nevertheless, functional
95 dependencies were obtained for a number of materials using this method^[25–29]. To cover the
96 parameter space in increments of 10° a set of GBs of approximately 6×10^3 is necessary for
97 cubic symmetry^[4]. Recently an update of the Morawiec method was proposed, where the
98 constrain of constant GB energy within each domain was removed^[30].

99 In this paper, we present a comprehensive analysis of a diverse set of GBs in a
100 polycrystalline sample. We have analyzed the dependence between the GBCD and GBED for
101 various subsets of the parameters used to describe the GB structure. It has been possible to
102 interpret the results in the framework of widely used theories, for example the theory of the
103 coincidence site lattice (CSL) and the dependence of the GB energy on the excess free
104 volume. In performing this study, we have found new phenomena such as the presence of an
105 energy minimum for GBs with plane orientation close to (101), a sufficient difference
106 between asymmetrical and symmetrical low index GBs, and the absence of any correlation
107 between GB population and energy. To provide atomistic insights and to ensure consistency
108 in the results, we have also calculated the energies for a similar number of symmetric tilt
109 GBs using the embedded atom method. We believe that our results will be used to construct
110 new extrapolation functions for GBED(GBCD) in future studies.

111 EXPERIMENT

112 An electrolytically deposited polycrystalline copper foil of 18 μm in thickness was used to
113 perform the experimental measurements. Disks of 3 mm in diameter were cut from the foil,
114 cleaned with acetone, and annealed in a quartz tube under dry hydrogen flux for 6 h at
115 1273 K. After the heat treatment, the tube with the sample was quenched in air with a cooling
116 rate between 100 and 200 K/min. The foil samples were characterized with a JSM-840A
117 scanning electron microscope equipped with an electron backscatter diffraction analyzer.
118 Orientation image microscopy[©] (OIM) maps with 3 μm of spatial resolution were obtained.

119 The foil surface was investigated using an optical interferometer MII-4 based on the Linnik
120 interference system. Dihedral angles ψ in the vicinity of the GB grooves were measured for
121 515 GBs using the following technique: The 3D profile of the foil surface, which contains
122 the GB trace (line of intersection between the GB plane and substrate surface), was
123 reconstructed from an interference image of the surface using the interferometer software.
124 Then, five 2D profiles were extracted from the 3D reconstruction for each GB groove
125 perpendicular to the sample surface and the GB trace on the surface. To extract the dihedral
126 angles (ψ), the 2D profiles were fitted using quadratic polynomials through the least squares
127 method (Fig. 1). The dihedral angle ψ between solid surfaces was calculated from an average
128 of five values, measured from the 2D profiles for a given GB. Dihedral angles were
129 measured at a distance of more than 5 μm from the GB triple junctions to avoid the effect of
130 GB groove deformation in the vicinity of the triple point due to the triple point line
131 tension^[31].



132

133 **Figure 1.** Optical micrograph of foil surface and 2D profile of grain boundary groove fitted with
 134 quadratic polynomials to extract dihedral angles ψ (see insert).

135 To estimate the total error of GB energy measurement, we used the standard technique,
 136 which involves a calculation of the average value and the error of the directly measured
 137 quantity (dihedral angle in the GB groove), followed by the estimation of the average value
 138 and the error of the indirectly measured quantity (GB energy). The absolute error of the
 139 dihedral angle measurement $\Delta\psi$ is defined as follows:

$$\Delta\psi = \frac{1}{n} \sum_{i=1}^n |\Delta\psi_i| \quad (1)$$

140

141 where $\Delta\psi_i$ are the residuals ($\Delta\psi_i = \psi_i - \langle\psi\rangle$) and n is the number of measurements for a
 142 given GB (5). Using a first-order Taylor series expansion, the absolute error of the GB
 143 energy measurement $\Delta\gamma_{GB}$ can be defined as follows:

$$\Delta\gamma_{gb} = \left| \frac{\partial\gamma_{gb}}{\partial\psi} \Delta\psi \right| \quad (2)$$

144

145 By considering the relationship between the GB energy and the solid/liquid interface energy
 146 (Eq. 6), and the relative error equation ($\epsilon_{Y_{GB}} = \Delta Y_{GB} / \langle Y_{GB} \rangle$), the final expression for relative
 147 error of the GB energy measurement $\epsilon_{Y_{GB}}$ is equal to

$$\varepsilon_{Y_{gb}} = \frac{1}{2} \tan(\psi) \Delta\psi \quad (3)$$

148

149 Thus, the relative error of the GB energy measurement is a nonlinear function of the dihedral
 150 angle. For instance, the relative error $\varepsilon_{Y_{GB}}$ reaches 0.3 % with a value of $\psi = 175^\circ$ and it
 151 equals just 0.1 % for $\psi = 165^\circ$ (the average dihedral angle for all GBs considered).

152 The error of the instrument is determined by $\frac{\lambda}{2NR}$, where λ is the wavelength of the light
 153 source (650 nm), N is the number of treated interference images, and R is a bit depth of the
 154 interference images used for profile reconstruction (256). This quantity is negligible
 155 compared to the above-considered random error.

156 Only straight fragments of GB traces were analyzed to minimize the variation of the GB
 157 plane orientation within the same boundary. The orientation of GB traces with respect to the
 158 sample coordinate system was obtained for 515 GBs. Inspection of the sample surface from
 159 both sides reveals that the copper foil has a columnar grain structure with an average grain
 160 size of approximately 30 μm (previously reported, Fig. 1a in ref.^[32]). It is assumed that the
 161 GB planes are perpendicular to the sample surface as their inclination is less than 10° ^[32].

162 Both the dihedral angles ψ and the five macroscopic degrees of freedom were obtained for all
 163 515 GBs in the copper foil. Results are compared with those in previous reports on
 164 GBED(GBCD) relationships in copper and with molecular statics simulations performed for
 165 symmetrical tilt GBs.

166 MODELING

167 To investigate the properties of GBs computationally, the energetic stability of 400
 168 symmetric tilt GBs (STGBs) in copper was computed. STGBs are special GBs between two
 169 different crystallographic orientations rotated in equal and opposite directions about a
 170 common tilt axis. The GB orientations are defined using Miller indices $(hkl)[mno]$, where
 171 (hkl) specifies the GB plane and $[mno]$ the tilt axis. Periodic supercells containing two
 172 symmetrically equivalent GBs were constructed using the bicrystal approach. The separation
 173 between the GBs was set to be greater than 30 \AA , which was found to be large enough
 174 considering that the mutual elastic interactions are small. Further details of the construction

175 of STGBs are included in ref.^[33]. The structure of the supercells is optimized using the
176 embedded atom method (EAM) description of the interatomic interactions. The total energy
177 of the EAM takes the following form:

$$E_{tot} = \frac{1}{2} \sum_{ij} V(r_{ij}) + \sum_i F_i(\rho(r_{ij})) \quad (4)$$

178
179 where $F(\rho)$ is the embedding function, ρ is the density, and V is the pairwise repulsion^{[34][35]}.
180 Here we use the parameterization of Ackland et al., which has been shown to yield very good
181 agreement with experiments for both the structure and associated properties (e.g.,
182 mechanical, electronic, or chemical)^[33,34,36–39].

183 To optimize the GBs, the γ surface method was used. This method finds the minimum total
184 energy of the system by performing a series of optimizations from different initial translation
185 states of the two grains relative to each other. The supercells are fully relaxed with respect to
186 the positions of all atoms and the length of the supercell in the GB normal direction. The GB
187 energy γ_{gb} is defined as

$$\gamma_{gb} = \frac{E_{tot} - NE_{coh}}{2A} \quad (5)$$

188
189 where E_{tot} is the total energy of the system, N is the number of atoms in the system, and
190 E_{coh} is the cohesive energy of the system. Comparison of GB energy values in copper
191 calculated as described above with values obtained from DFT calculations show divergence
192 up to 35%, relative stability of GBs predicted by EAM and DFT coincides^[33].

193 As there are only three degrees of freedom associated with an STGB, it is possible to perform
194 a mapping from the entire 3D space of possible boundaries to a 2D projection. The 2D
195 projection can then be interpolated to predict the GB energy of an arbitrary STGB. The 2D
196 projection can be intersected to describe all possible GB energy misorientation angles for
197 each different tilt angle. Plots for each specific GB energy/ misorientation are omitted but
198 can be found in the academic literature^[5,13]. More details of this approach can be found in the
199 appendices of ref.^[33].

200 RESULTS AND DISCUSSION

201 The statistical analysis of the grain orientation reveals a strong texture in the $\langle 110 \rangle$
 202 orientation normal to the foil^[32]. The same texture was also detected for electrodeposited
 203 copper in ref.^[21]. To analyze the relationship between GB energy and geometry, the GB
 204 energies were extracted from the experimentally measured dihedral angles ψ as follows:

$$205 \quad \gamma_{gb} = 2\gamma_{sg} \cos\left(\frac{\psi}{2}\right) \quad (6)$$

206 where γ_{gb} is the GB energy and γ_{sg} is the solid/gas surface energy. Eq. 6 can be used if the
 207 solid/gas surface energy γ_{sg} is isotropic. If the surface energy is anisotropic, then the Herring
 208 equation^[40], included below, should be used instead.

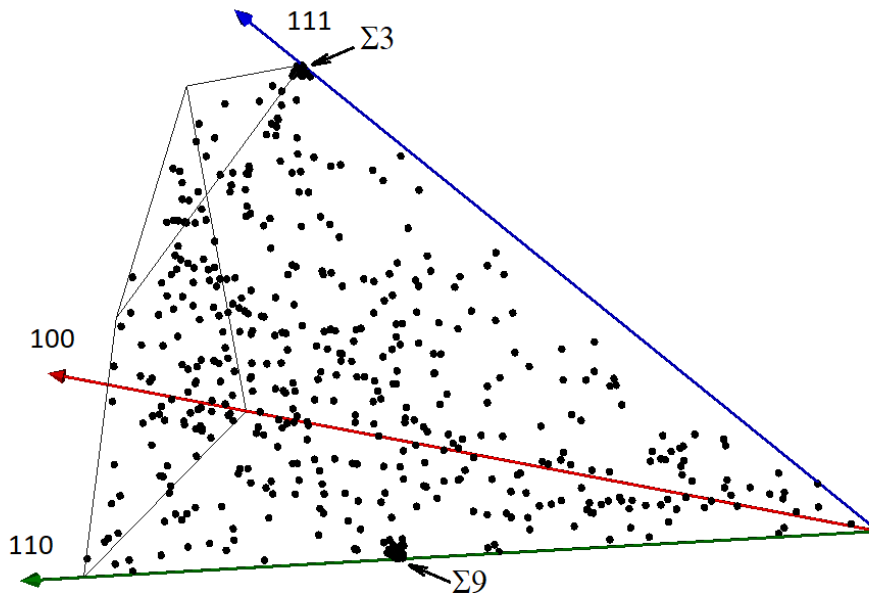
$$209 \quad \sum_{i=1}^3 \left(\bar{\epsilon}_i \gamma_i + (\bar{\epsilon}_i \times \bar{s}) \frac{\partial \gamma_i}{\partial \varphi_i} \right) = 0 \quad (7)$$

210 where γ_1 and γ_2 are the surface energies of copper crystals forming the planes in the GB, γ_3
 211 is the GB energy, and $\frac{\partial \gamma_i}{\partial \varphi_i}$ are the variations of the surface and GB energies with plane
 212 orientation (torque terms). The error introduced from the isotropic approximation can be
 213 estimated using anisotropy data of a solid copper surface from the work of D. Chatain et
 214 al.^[41]. The main result of the Chatain study is presented in the so called γ -plots, where the
 215 variance of the crystal surface energy is given. Owing to the presence of the $\{110\}$ texture in
 216 our sample^[32], we can estimate the maximum values of $\frac{\partial \gamma_{sg}}{\partial \varphi_i}$ from the maximum gradient of
 217 the γ -plot close to the $\{110\}$ plane (see Fig. 6 in ref.^[41]). This estimation gives
 218 $\frac{\partial \gamma_{sg}}{\partial \varphi_i} \leq 19 \text{ mJ/m}^2$, which is approximately 5 % of the average GB energy. To estimate the
 219 contribution of torque terms $\frac{\partial \gamma_{sg}}{\partial \varphi_i}$ into γ_{gb} values, Eq. 7 can be simplified to the scalar form
 220 for a symmetrical GB groove,

$$221 \quad \gamma_{gb} = \gamma_1 \cos\left(\frac{\psi}{2}\right) + \gamma_2 \cos\left(\frac{\psi}{2}\right) + \left(\pm \frac{\partial \gamma_1}{\partial x} \pm \frac{\partial \gamma_2}{\partial x} \right) \sin\left(\frac{\psi}{2}\right) \quad (8)$$

222 If we neglect torque terms $\frac{\partial \gamma_{sg}}{\partial \varphi_i}$ in the calculation of GB energy from the dihedral angle and
 223 reduce Eq. 8 to Eq. 6, we obtain a maximum error of 38 mJ/m² (approximately 9 % of the

224 average GB energy in our sample). As we have estimated previously ^[42] the average value of
 225 torque term $\frac{\partial \gamma_{gb}}{\partial \varphi_i}$ in copper foil is less than 20% of average GB energy. If we neglect it in the
 226 case of columnar structure and isotropic surface energy the error in GB energy determination
 227 could be estimated as follows: $\sqrt{1 + \left(\frac{\partial \gamma_{gb}}{\partial \varphi_i} / \gamma_{gb}\right)^2} - 1$, which is less than 2%. The above
 228 considerations allows us to use the relation (Eq. 6) to calculate GB energies. γ_{sg} is estimated
 229 for 970°C, and is equal to 1650 mJ/m²^[43], which is in good agreement with data from other
 230 sources^[44]. The number of GBs studied did not allow us to reveal all the local energy minima
 231 in the GBED, but trends for specific subsets of the macroscopic parameters have been found.
 232 The range of misorientations is presented in the fundamental zone of Rodrigues-Frank
 233 space^[45] (Fig. 2). It can be observed in Fig. 2 that the misorientation space is filled with
 234 experimental points more or less uniformly, with a slightly higher density of points near $\Sigma 3$
 235 and $\Sigma 9$ GBs.

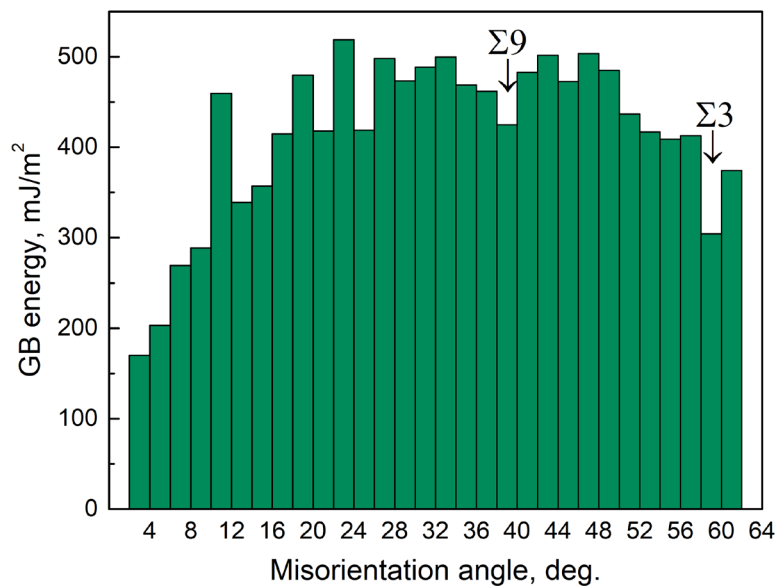


236
 237 **Figure 2.** The 515 experimentally determined misorientations represented in the fundamental zone
 238 of Rodrigues-Frank space.

239
 240 The copper foil under investigation has a pronounced $\langle 110 \rangle$ texture, and the GB planes are
 241 oriented perpendicular to the foil surface. Only $\Sigma 3$, $\Sigma 9$, and $\Sigma 27$ GBs occurred more
 242 frequently in the foil than in the simulated set of GBs, which confirms a special to general

243 structural transition at the annealing temperature for other CSL misorientations^[46]. An
 244 analysis of the tilt-to-twist relation did not reveal any specific features compared with a
 245 randomly generated GB set, except that the tilt boundaries are enriched due to twinning^[32].
 246 GB plane orientation statistics were also analyzed, and it was found that $\{111\}$ planes were
 247 significantly enriched, which can be explained by the foil texture (Fig. 3 in ref.^[32]). When
 248 compared to a random distribution of grains in an arbitrary cubic crystal, the probabilities of
 249 finding GB planes in a $\langle 110 \rangle$ textured foil are 1/2 for $\{111\}$, 1/3 for $\{100\}$, and 1/6 for
 250 $\{110\}$.

251 We discuss the effect of GB misorientation (3 DOF) and GB plane orientation (2 DOF)
 252 separately. The most straightforward approach is to plot the GB energy vs misorientation
 253 angle, ignoring the four other macroscopic DOFs. Rotation by the misorientation angle
 254 allows the superposition of elementary cells of adjacent grains; the rotation axis is selected so
 255 that the value of the misorientation angle is minimized, thus positioning a given
 256 misorientation in the fundamental zone (as shown in Fig. 3). $\Sigma 3$ and $\Sigma 9$ GBs are located at
 257 60° and 38.9° correspondingly, but 38-40 and 58-60 column charts contain also general GBs.



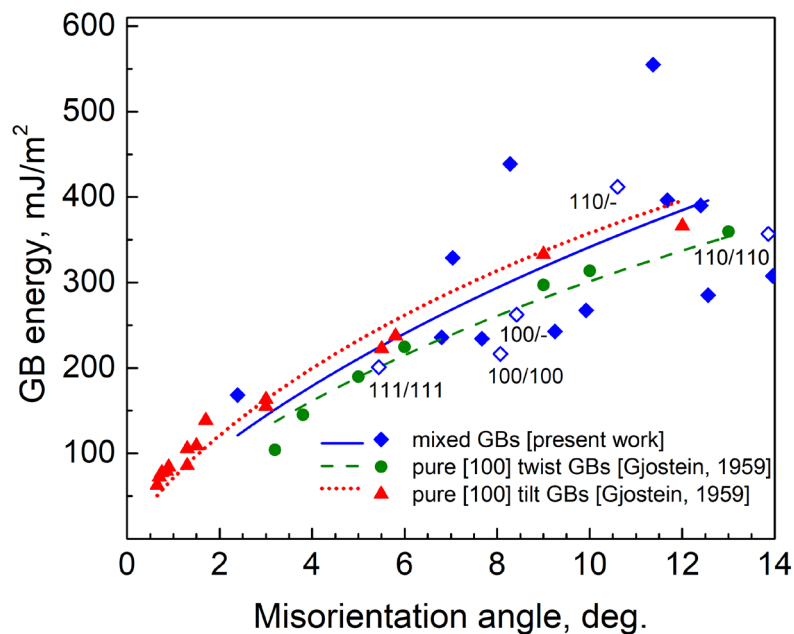
258

259 **Figure 3.** Grain boundary energy vs misorientation angle for the copper foil studied in this work.

260

261 The effect of GB plane orientation is determined through the analysis of tilt and twist
 262 components. An additional parameter is the angle $\angle(\omega, \nu)$ between the rotation axis ω
 263 and the GB plane normal ν ^[47]. When $\angle(\omega, \nu)$ is equal to 0° , it is a pure twist boundary, and when
 264 it is equal to 90° , it is a pure tilt boundary. Boundaries with $0^\circ < \angle(\omega, \nu) < 90^\circ$ are known
 265 as mixed.

266 For most misorientations, the average GB energy is constant with a reduction towards angles
 267 less than 15° . A quantitative description of the GB energy/misorientation relationship in
 268 small angle GBs based on dislocation models was proposed by Read and Shockley^[9]. The
 269 Read--Shockley model was quantitatively confirmed using highly symmetrical pure tilt or
 270 twist GBs and is used to predict energies in pure tilt and twist systems^[15]. It is difficult to
 271 present mixed GBs as a systematic array of dislocations. An attempt to fit our data with the
 272 Read--Shockley equation was made, but in this work, most of the low angle GBs are mixed.
 273 We have plotted the GB energy of the low angle GBs in our sample together with data for
 274 highly symmetrical GBs from ref.^[15] (Fig. 4). All the data are fitted with the Read-Shockley
 275 equation.

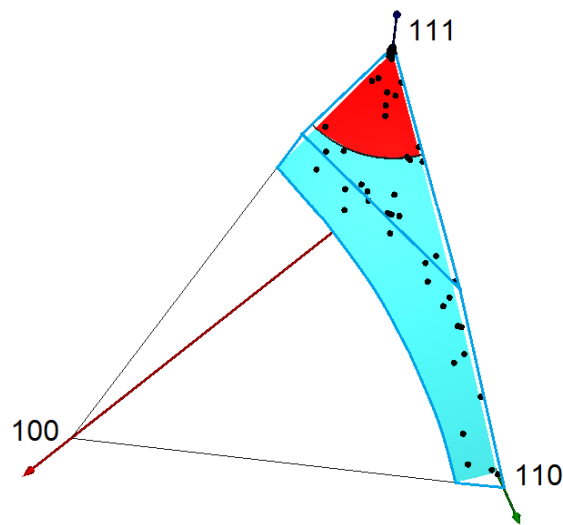


276

277 **Figure 4.** Grain boundary energy of low angle grain boundaries of mixed type (copper foil, 1000° ,
 278 this study) compared with grain boundary energy of low angle **[100]** tilt and twist grain boundaries
 279 in copper bicrystals at 1065° ^[15].

280

281 The average GB energies for mixed tilt/twist boundaries (our data, blue line) are located
282 between the energies of tilt and twin boundaries determined in ref.^[15]. There is a spread of
283 GB energies of approximately hundreds of mJ/mol for mixed GBs, which is much larger than
284 the spread of the energies found in ref.^[15] for pure tilt and twist GBs. Our data consists of
285 seventeen GBs with a misorientation angle less than 15° , including three GBs with two low
286 index GB planes, two GBs with one low index plane (empty rhomb), and 12 GBs without
287 low index GB planes (filled rhombs). A low index plane was attributed to a GB if the
288 deviation between the experimentally obtained plane orientation and the low index plane was
289 less than 10° . GBs with two low index planes have relatively low energies, but GBs with
290 only one low index plane have higher energies. The majority of GBs investigated did not
291 contain low index planes, including those with an energy considerably lower than the
292 average value predicted by the Read-Shockley model.

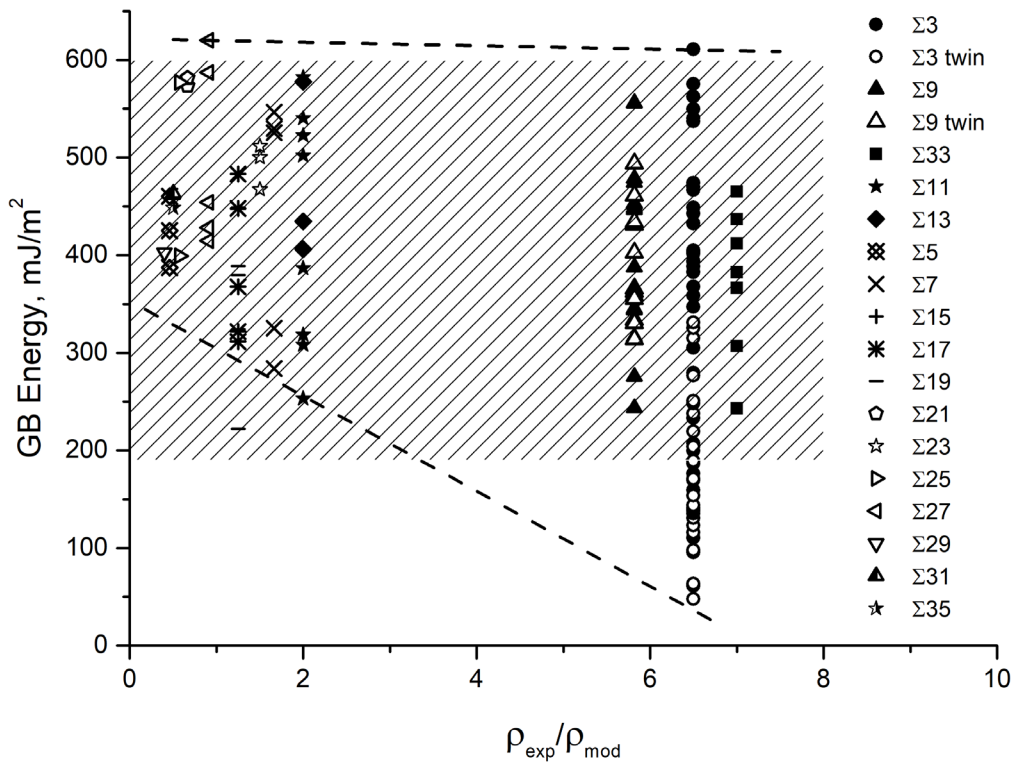


293

294 **Figure 5.** Grain boundaries with misorientation angle 58° – 62.8° in Rodrigues-Frank space. The
295 points in the red zone correspond to $\Sigma 3$ according to the Brandon criterion ($\theta_0 = 15^\circ$).

296 For high angle GBs, the energy vs misorientation distribution is smooth, except for two mild
297 minima. One minimum is close to 39° and could be linked to the presence of $\Sigma 9$ GBs and the
298 other minimum is close to 60° , which corresponds to $\Sigma 3$ GBs. The presence of mild minima
299 close to 39° and 60° is linked to the presence of special (in terms of CSL) GBs. Special GBs
300 in terms of the CSL model (GBs with $\leq \Sigma 35$) were selected from the experimental data set.

301 The Brandon criterion^[48] ($\theta_0 = 15^\circ/\sqrt{\Sigma}$) was used to classify GB as “special.” A total of
 302 68 % of GBs were identified as $\Sigma 3$ in the 58° – 62.8° misorientation angle range. These GBs
 303 are presented as points inside a polygon limited by thick blue lines in the Rodrigues-Frank
 304 space (see Fig. 5). In total, 40 % of GBs were identified as $\Sigma 9$ in the 37° – 41° misorientation
 305 angle range (see Fig. 3). $\Sigma 3$ and $\Sigma 9$ GBs have an average energy value lower than general
 306 GBs, and the average $\Sigma 3$ energy is lower than $\Sigma 9$.

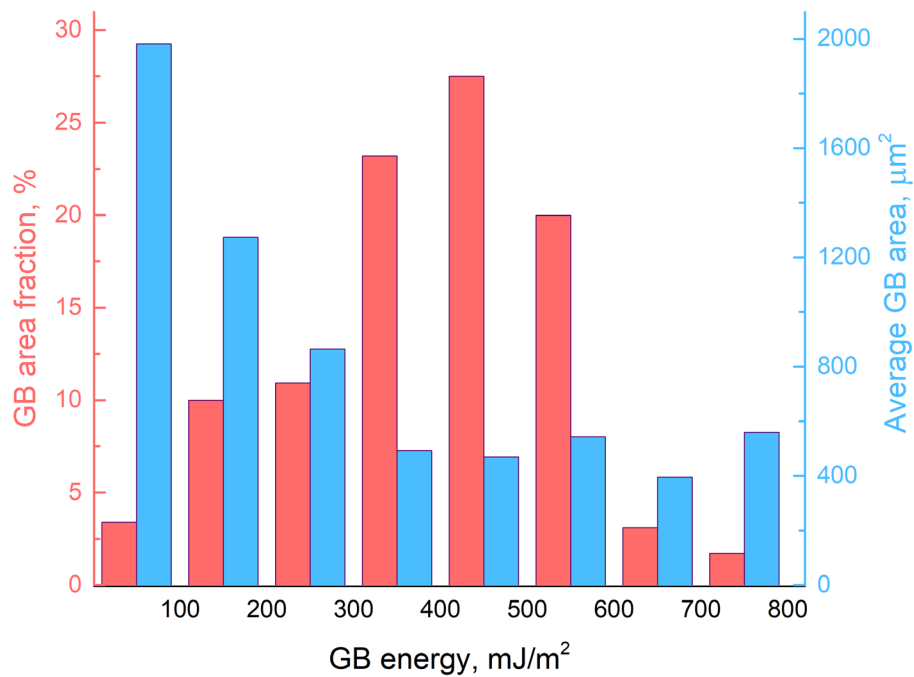


307

308 **Figure 6.** Dependence of grain boundary energy and frequency of occurrence, which is normalized
 309 by the frequency generated from random simulation accounting for foil texture. Full range of general
 310 grain boundary energy is denoted by hatched area.

311 The energy of special GBs in terms of the CSL model is plotted against the frequency of their
 312 occurrence (ρ_{exp}) in Fig. 6. The frequency of occurrence (ρ_{exp}) was normalized by the
 313 frequency of occurrence for the same misorientations in the simulated set of GBs (ρ_{mod}).
 314 Grain orientations in ρ_{mod} were generated by considering the $\langle 110 \rangle$ texture of the copper
 315 foil^[32]. During the microstructure inspection, twins were identified within $\Sigma 3$ and $\Sigma 9$ GBs,
 316 and they are marked by open cycles and open triangles, respectively. Despite the high
 317 occurrence frequency for $\Sigma 3$, $\Sigma 9$, and $\Sigma 33$ GBs, only $\Sigma 3$ twins have a significantly lower GB

318 energy. The energy of the other special GBs is not significantly different from the energy of
 319 GBs with no Σ value assigned (only $\leq \Sigma 35$ were considered). Such GBs should be considered
 320 as general in terms of CSL formalism. The result that $\Sigma 3$ GBs have a lower energy is in good
 321 agreement with the hypothesis of “special GBs transition to general ones with increasing
 322 annealing temperature^[46].” During recrystallization annealing of the copper foil, abnormal
 323 grain growth was not observed; thus, the misorientation statistics are close to those of a
 324 copper foil with a random distribution of grains taking into account the presence of texture.
 325 The sharp increase in $\Sigma 3$ and $\Sigma 9$ boundaries could be attributed to the stability of these
 326 boundaries during recrystallization, and they decrease in number more slowly than high
 327 energy GBs. It should be noticed that number density of $\Sigma 9$ boundaries (0.062) exceed
 328 probability of two $\Sigma 3$ boundaries meeting ($0.126^2 = 0.016$). Similarly, number density of $\Sigma 33$
 329 GBs (0.0136) exceed probability of $\Sigma 3$ and $\Sigma 11$ meeting ($0.126 * 0.0155 = 0.002$)^[49].



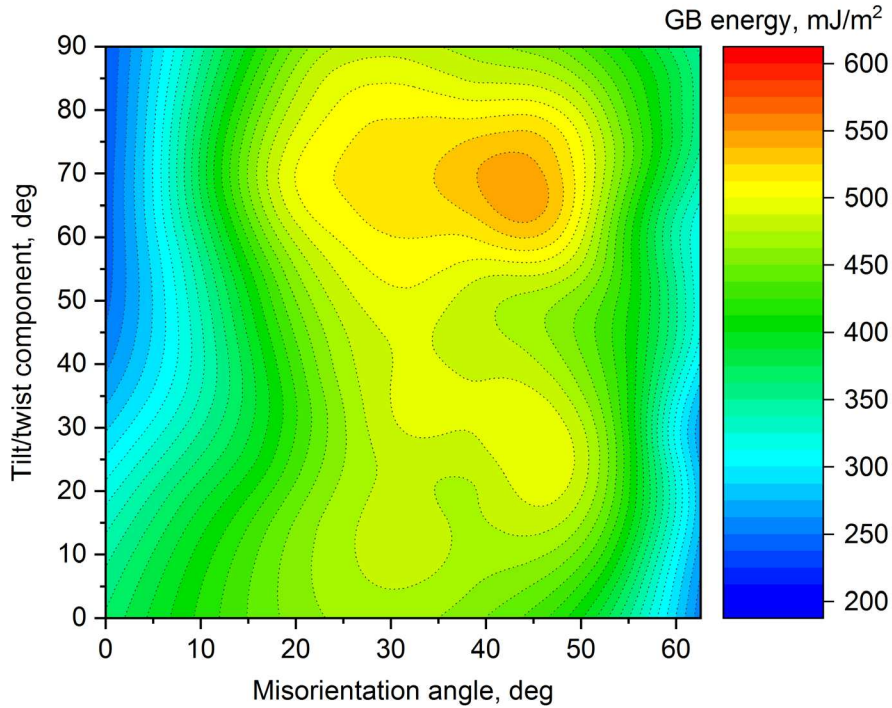
330

331 **Figure 7.** Correlation between the total grain boundary area (red) of each grain boundary fraction
 332 and the average area of a single GB (blue) in the corresponding grain boundary energy range.

333 A strong linear correlation between GB energy and population was reported for
 334 polycrystalline nickel^[24] and magnesium oxide^[6]. A similar correlation was not observed in

335 the copper foil investigated in this study. It can be observed in Fig. 7 (red) that the maximum
336 GB area fraction corresponds to GBs with an average energy. The distribution in Fig. 7 is
337 asymmetric as GBs with the lowest energy are more frequent than GBs with the highest
338 energy. Such asymmetric behavior can be linked to the grain structure of the copper foil. The
339 area distribution is not in equilibrium and is caused by the initial foil texture.
340 Recrystallization of the copper foil did not lead to a significant structural relaxation towards
341 GBs with a lower surface energy despite 6 h annealing at 1000°C. We believe that the
342 recrystallization is linked to the specific morphology of the foil with $\{110\}$ texture. For
343 example, in a textured thin film with a columnar structure, not all GB geometries are
344 possible. Those that do occur are relatively more stable than in a 3D polycrystalline sample.
345 During crystallization, the area of the individual boundary grows if the GBs have a low
346 energy and decreases if the GBs have a high energy. This results in the distribution of
347 individual GB areas presented in (Fig. 7).

348 The misorientation angle alone is not sufficient to describe the energy/misorientation
349 relationship, especially for high angle GBs. A tilt/twist relation defined as the angle between
350 the GB plane normal and the GB misorientation axis was previously suggested as an
351 additional misorientation parameter^[16,47]. It was demonstrated in ref.^[47] that in FeSi alloys,
352 twist GBs have a higher adsorption capacity for Si atoms. The Krakauer result is in
353 agreement with experimental data presented in ref.^[16] where twist GBs have an average
354 energy higher than that of the tilt ones in a NiAl intermetallic polycrystal. In some special
355 cases, twist boundaries were found to have lower energy than tilt GBs with the same
356 misorientation^[15].

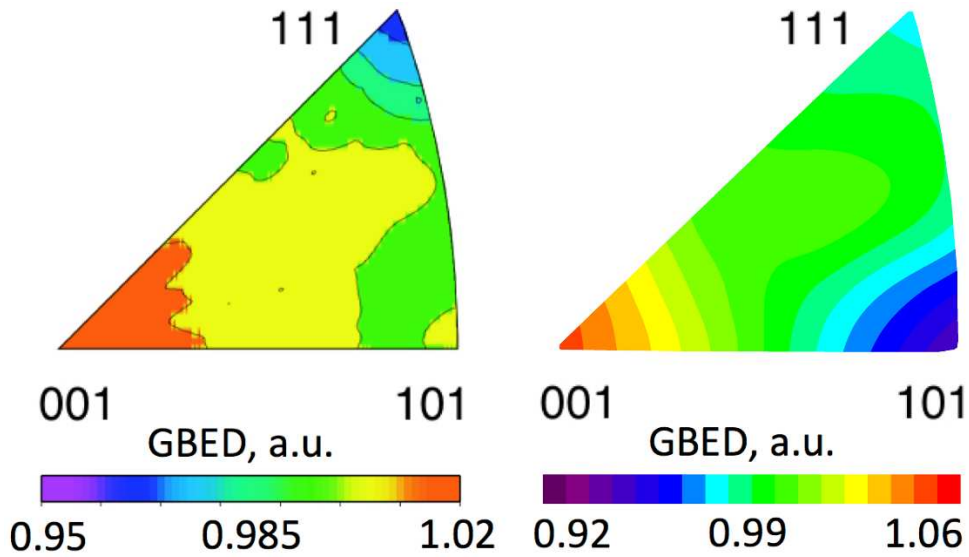


357

358 **Figure 8.** Grain boundary energy as a function of misorientation angle and tilt/twist relation for
 359 copper foil.

360

361 Variation of the GB energy in the copper foil with a tilt/twist relation and misorientation
 362 angle is presented in Fig. 8. The experimental data is fitted with a smooth surface. Low
 363 energy GBs are observed at a low misorientation angle and close to 60° misorientation (due
 364 to $\Sigma 3$ $\{111\}/\{111\}$ GBs) independent of the tilt/twist relation. At the same time, twist GBs
 365 have a slightly lower energy in the entire misorientation range. The region of GBs with the
 366 highest energy is situated between 30° and 45° misorientation and at $\angle(\omega, \nu) = 60^\circ - 80^\circ$.
 367 The result of the ranges of angles is in general agreement with experimental data for
 368 symmetrical GBs^[15] and with the molecular statics simulation of GB energy^[6]. The
 369 difference between the GB energy of predominantly tilt and predominantly twist GBs is quite
 370 weak. This is in agreement with GB statistical data^[32].



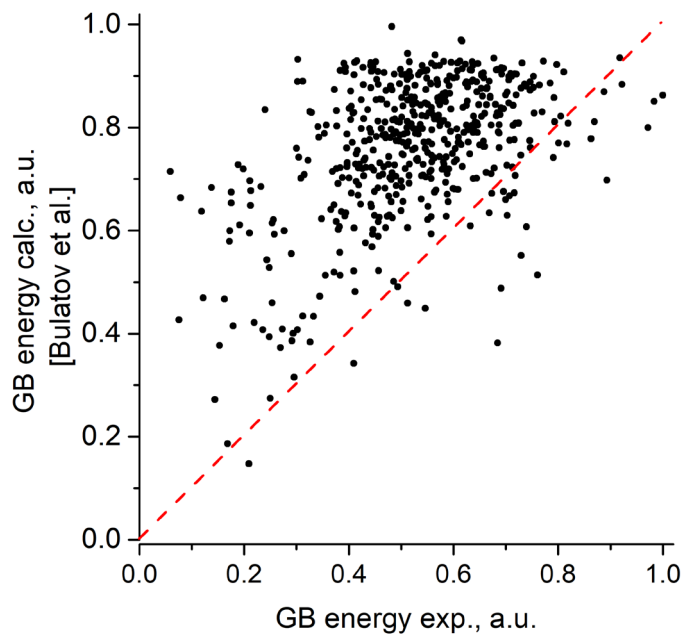
371

372 **Figure 9.** (left) Grain boundary energy distribution as a function of grain boundary plane orientation
 373 for nickel^[4] (the figure was kindly provided by Prof. G.S. Rohrer, Carnegie Mellon University) and
 374 (right) copper (this work).

375 The influence of GB plane orientation on the GB energy is well established^[50,51]. To analyze
 376 the GB plane orientation in our copper foil, the GB energy relationship for a large set of
 377 mixed GBs in the polycrystal was measured to plot GB energy vs GB plane orientation
 378 relative to the crystal lattice of adjacent grains in the form of an azimuthal projection (for
 379 example^[27]). In the azimuthal projection, each GB is counted twice and misorientation of
 380 grains is partially ignored. For example, if one grain is rotated around a GB plane normal, we
 381 will obtain different GBs with a similar orientation of the GB plane. In Fig. 9, we compare
 382 our data for the copper foil with a similar representation in a nickel polycrystal^[4] by means of
 383 the Morawiec method^[52]. In both cases, copper and nickel, a minimum is observed near the
 384 $\{111\}$ orientation meaning that $\Sigma 3$ GBs with a low GB energy make a significant
 385 contribution into the average GB energy. It is also found that an increase in GB energy is
 386 observed for GB plane orientations close to $\{100\}$ in both copper and nickel. The most
 387 important difference between copper and nickel is for GBs close to $\{110\}$: in the case of
 388 nickel, there is no noticeable deviation from the average GB energy value, whereas for
 389 copper foil a pronounced minimum was observed.

390 The variation of the range of average GB energies with plane orientation is insignificant
 391 when considering that GB energies vary by more than an order of magnitude depending on

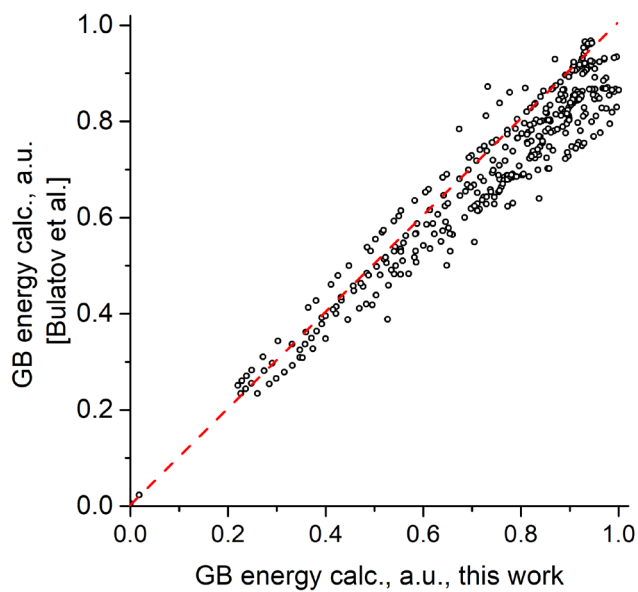
392 misorientation. In our opinion, considering the GB plane orientations without taking into
393 account grain misorientation will not reveal sharp energy minima in fcc metals. Moreover,
394 the approach described above did not make any distinction between symmetrical and
395 asymmetrical GBs.



396

397

(a)



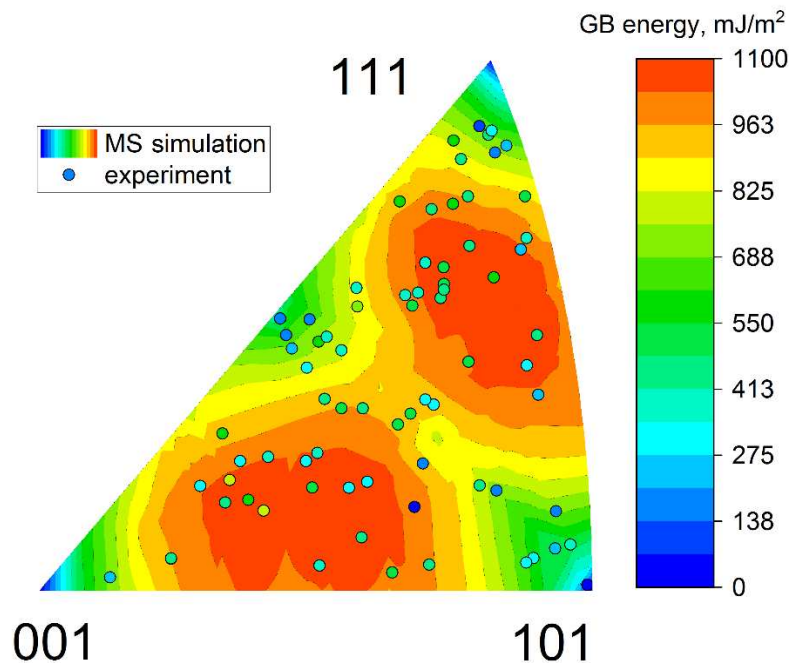
398

399

(b)

400 **Figure 10.** GB energy values calculated by the function developed in ref.^[8] vs those obtained from
401 the experiment with copper foil (a) and calculated by means of molecular statics in this work (b).

402 It is difficult to cover the 5D space with experimental data, and thus, it is desirable to build a
403 function that determines the GB energy for each misorientation. Recently, a 5DOF function
404 aimed at reconstructing the GBED(GBCD) relationship was suggested^[8]. The new 5DOF
405 method uses the energies of 388 GBs in four fcc metals calculated from atomistic simulations
406 using EAM potentials as reference points^[6]. GBs considered by Olmsted et al. have periodic
407 length for each grain no more than $15a_0/2$, where a_0 is the lattice spacing. In the present work,
408 we have calculated energies for all GBs from their geometrical parameters using the function
409 developed in ref.^[8]. The correlation between the GB energy calculated from dihedral angles
410 ψ in the vicinity of GB grooves and the approximation function of Bulatov et al. (Fig. 10a) is
411 very weak. A similar weak correlation between the experimental and theoretical predictions
412 was observed for nickel^[24]. For general GBs in nickel, the correlation between the GB
413 energies simulated in ref.^[6] and those determined experimentally in ref.^[27] was not observed.
414 Comparison of GB energy values, calculated by molecular statics in this study with values
415 calculated for the same GB parameters by the function presented in ^[8] is presented in Fig
416 10b. Good correlation is observed in agreement with the fact that in both cases GBs with
417 short period were modelled.



418

419 **Figure 11.** Azimuthal projection of GB plane orientation for 74 symmetrical GBs selected from the
 420 experimental data set (cycles) superimposed with GBED obtained by smoothing of molecular statics
 421 (MS) calculated values of GB energies for 400 symmetrical tilt GBs in copper.

422 As presented in Table. 1, GBs that are close to low index planes for one grain only ($\{111\}$,
 423 $\{100\}$, and $\{110\}$ asymmetrical GBs) have an energy close to the average GB energy. On the
 424 contrary, for symmetrical $\{100\}/\{100\}$, $\{111\}/\{111\}$, and $\{110\}/\{110\}$ GBs, there is a
 425 significant decrease in average GB energy. Even in the $\{100\}/\{100\}$ case (there is only one
 426 GB of this type, and thus, it is not representative), the GB energy is 1/2 the average GB
 427 energy. The energy of GBs combined from different low index planes is higher than the
 428 energy of symmetric GBs. Only the $\{100\}/\{110\}$ GB demonstrates relatively low energy,
 429 but only one GB of this type was found experimentally.

430 Table 1: Average GB energies and their fraction in the studied GB ensemble for
 431 asymmetrical and symmetrical low index GBs in copper foil. Indexes were attributed to the
 432 GB plane if its deviation from the given orientation was less than 10° .

GB plane indexes	$\{100\}/-$	$\{111\}/-$	$\{110\}/-$
$\gamma_{gb} / \gamma_{av}$	1.06	1.08	0.97
Fraction of GBs, %	10.2	11.1	10.5
GB plane indexes	$\{100\}/\{100\}$	$\{111\}/\{111\}$	$\{110\}/\{110\}$
$\gamma_{gb} / \gamma_{av}$	0.51	0.62	0.66
Fraction of GBs, %	0.2	1.6	2.0
GB plane indexes	$\{111\}/\{100\}$	$\{111\}/\{110\}$	$\{100\}/\{110\}$
$\gamma_{gb} / \gamma_{av}$	0.93	1.11	0.72
Fraction of GBs, %	2.0	2.0	0.2

433

434 The GBED calculated by smoothing of the simulation data for 400 STGBs in copper and the
 435 experimental data for a subset of symmetrical GBs from the copper foil are presented in
 436 Fig. 11. There is a good agreement between the experimental data and simulation. The
 437 simulation demonstrates the presence of four pronounced energy minima close to the $\{111\}$,
 438 $\{100\}$, $\{110\}$, and $\{311\}$ GB planes. These minima correlate with the decrease in free excess

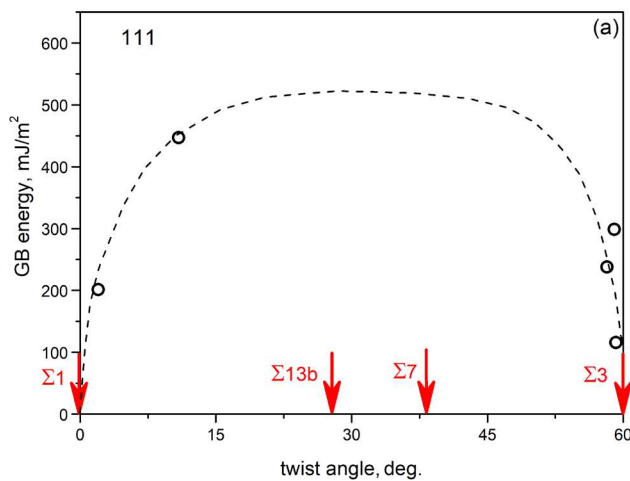
439 volume, as was previously reported^[50]. The experimental data show the same tendency with
440 additional variance and several exceptions. The exceptions are likely related to the inclusion
441 of twist components, which are ignored using this representation. In addition, larger values of
442 GB energy are obtained from the simulation and could relate to the temperature difference
443 (the simulation corresponds to 0 K, whereas the experiment was performed at 1273 K).

444 For the {111}, {110}, and {311} GB planes, the effect of twist is shown in Fig. 12. It can be
445 observed in Fig. 12 that the twist component has a significant influence on the energy of
446 symmetrical GBs. The most pronounced minima align with the special CSL misorientations
447 $\Sigma 3$ and $\Sigma 9$, which is similar for the entire set of studied copper GBs.

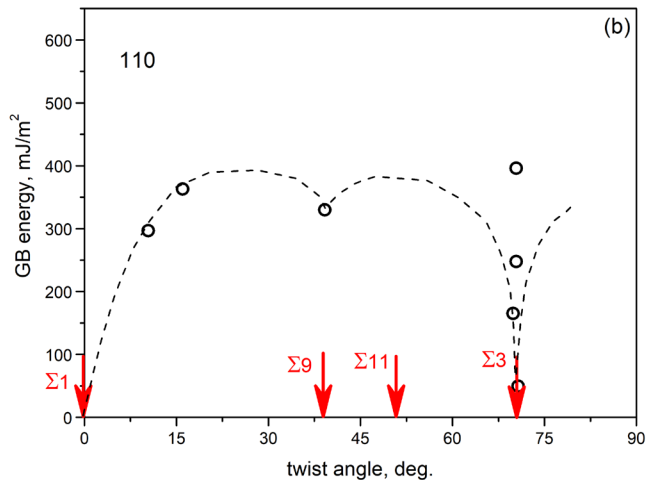
448 CONCLUSIONS

449 From the work presented in this paper, we can draw several conclusions. First, even for a
450 simple one-component fcc material, a universal relationship between GB energy and GB
451 macroscopic structure is far from being found. Second, in our work, we have identified new
452 subsets of low energy GBs (symmetrical $\{311\}/\{311\}$ and $\{110\}/\{110\}$), hence identifying
453 possible avenues to improve the agreement between experiment and theory.

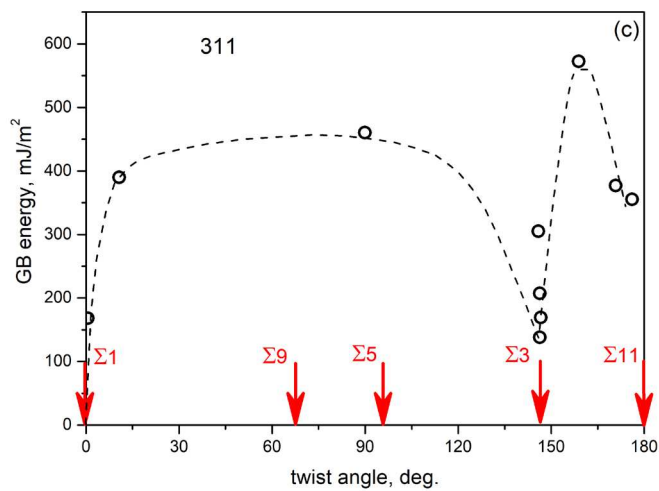
454



455



456



457

458 **Figure 12.** Grain boundary energy for symmetrical GBs vs twist angle for (a) $\{111\}$, (b)
 459 $\{110\}$, and (c) $\{311\}$ orientations. Deviation from the low index plane is less than 6° for all
 460 the presented points.

461

462 To explore the GBED(GBCD) relationship, we have consequentially increased the number of
 463 fixed macroscopic degrees of freedom. For example, if we draw energy as a function of
 464 misorientation angle (one fixed parameter, Fig. 3) or plane orientation (two fixed parameters,
 465 Fig. 9) for our copper foil, it is very difficult to interpret the complexity of the
 466 GBED(GBCD) relationship. However, pronounced GB energy minima could be revealed for
 467 a subset of symmetrical GBs (four fixed parameters, Fig. 11) and for a subset of symmetrical
 468 GBs with a fixed plane orientation as a function of twist angle (five fixed parameters,
 469 Fig. 12). This approach minimizes the set of possible assumptions about the functional

470 dependence between GB energy and its structure. An alternative strategy based on an
471 analytical approximation of the GBED(GBCD) landscape requires a representative set of
472 high-quality data.

473 The determination of GB energy and excess volume using first-principles calculations within
474 the framework of the density functional theory may provide an adequate base for
475 constructing the energy-structure function. Furthermore, usually GB energies are calculated
476 at 0 K in simulation, and thus, it could be that the calculation of the GB energy at finite
477 temperatures may yield a better relationship between simulation and experiment. At the same
478 time, first-principles calculations are notoriously time consuming and could not be used to
479 reconstruct the full 5-dimensional GBED(GBCD) relationship at the present moment. The
480 data obtained by molecular statics simulation for STGBs are in a good agreement with these
481 experimental findings and understanding the asymmetric effect of GBs could be a
482 compelling follow-on study.

483 ACKNOWLEDGEMENTS

484 This work was supported by the Russian Scientific Foundation under grant 19-72-10160. We
485 would also like to acknowledge the financial support from the EPSRC (EP/K003151) and the
486 support from the N8 Consortium (Polaris supercomputer) and the Materials Chemistry
487 Consortium (Archer supercomputer, EPSRC grant EP/L000202). We would also like to
488 acknowledge that part of this work was performed using resources provided by the
489 Cambridge Service for Data Driven Discovery (CSD3) operated by the University of
490 Cambridge Research Computing Service (<http://www.csd3.cam.ac.uk/>), by Dell EMC and
491 Intel using Tier-2 funding from the EPSRC (capital grant EP/P020259/1), and by DiRAC
492 with funding from the STFC (www.dirac.ac.uk). We give special thanks to Prof A. Lindsay
493 Greer for the useful discussion.

494

495

496 1 T. Watanabe: *J. Mater. Sci.*, 2011, vol. 46, pp. 4095–115.

497 2 V. Randle: *Acta Mater.*, 1998, vol. 46, pp. 1459–80.

498 3 V. Randle and G. Owen: *Acta Mater.*, 2006, vol. 54, pp. 1777–83.

499 4 G.S. Rohrer: *J. Mater. Sci.*, 2011, vol. 46, pp. 5881–95.

500 5 D. Wolf and S. Phillpot: *Mater. Sci. Eng. A*, 1989, vol. 107, pp. 3–14.

501 6 D.L. Olmsted, S.M. Foiles, and E.A. Holm: *Acta Mater.*, 2009, vol. 57, pp. 3694–703.

502 7 E.A. Holm, D.L. Olmsted, and S.M. Foiles: *Scr. Mater.*, 2010, vol. 63, pp. 905–8.

503 8 V. V. Bulatov, B.W. Reed, and M. Kumar: *Acta Mater.*, 2014, vol. 65, pp. 161–75.

504 9 W.T. Read and W. Shockley: *Phys. Rev.*, 1950, vol. 78, p. 275.

505 10 O.B.M. Hardouin Duparc: *J. Mater. Sci.*, 2011, vol. 46, pp. 4116–34.

506 11 P.R.M. Van Beers, V.G. Kouznetsova, M.G.D. Geers, M.A. Tschopp, and D.L.
507 McDowell: *Acta Mater.*, 2015, vol. 82, pp. 513–29.

508 12 L. Zhang, Y. Gu, and Y. Xiang: *Acta Mater.*, 2017, vol. 126, pp. 11–24.

509 13 J. Hickman and Y. Mishin: *Phys. Rev. Mater.*, 2017, vol. 1, p. 010601.

510 14 T. Frolov, D.L. Olmsted, M. Asta, and Y. Mishin: *Nat. Commun.*, 2013, vol. 4, pp.
511 1897–9.

512 15 N.A. Gjostein and F.N. Rhines: *Acta Metall.*, 1959, vol. 7, pp. 319–30.

513 16 Y. Amouyal, E. Rabkin, and Y. Mishin: *Acta Mater.*, 2005, vol. 53, pp. 3795–805.

514 17 Y. Amouyal and E. Rabkin: *Acta Mater.*, 2007, vol. 55, pp. 6681–9.

515 18 S.J. Dillon, M.P. Harmer, and G.S. Rohrer: *J. Am. Ceram. Soc.*, 2010, vol. 93, pp.
516 1796–802.

517 19 D.W. Hoffman and J.W. Cahn: *Surf. Sci.*, 1972, vol. 31, pp. 368–88.

518 20 J.L. Cahn and D.L. Hoffman: *Acta Metall.*, 1974, vol. 22, pp. 1205–14.

- 519 21 S. Ratanaphan, D. Raabe, R. Sarochawikasit, D.L. Olmsted, G.S. Rohrer, and K.N. Tu:
520 *J. Mater. Sci.*, 2017, vol. 52, pp. 4070–85.
- 521 22 M.A. Linne, T.R. Bieler, and S. Daly: *Int. J. Plast.*, 2020, vol. 135, p. 102818.
- 522 23 S.G. Baird, E.R. Homer, D.T. Fullwood, and O.K. Johnson: *Comput. Mater. Sci.*, 2021,
523 vol. 200, p. 110756.
- 524 24 G.S. Rohrer, E.A. Holm, A.D. Rollett, S.M. Foiles, J. Li, and D.L. Olmsted: *Acta*
525 *Mater.*, 2010, vol. 58, pp. 5063–9.
- 526 25 D.M. Saylor, A. Morawiec, and G.S. Rohrer: *Acta Mater.*, 2003, vol. 51, pp. 3675–86.
- 527 26 S.J. Dillon and G.S. Rohrer: *J. Am. Ceram. Soc.*, 2009, vol. 92, pp. 1580–5.
- 528 27 J. Li, S.J. Dillon, and G.S. Rohrer: *Acta Mater.*, 2009, vol. 57, pp. 4304–11.
- 529 28 H. Beladi and G.S. Rohrer: *Acta Mater.*, 2013, vol. 61, pp. 1404–12.
- 530 29 H. Beladi, N.T. Nuhfer, and G.S. Rohrer: *Acta Mater.*, 2014, vol. 70, pp. 281–9.
- 531 30 Y. Shen, X. Zhong, H. Liu, R.M. Suter, A. Morawiec, and G.S. Rohrer: *Acta Mater.*,
532 2019, vol. 166, pp. 126–34.
- 533 31 B. Zhao, J.C. Verhasselt, L.S. Shvindlerman, and G. Gottstein: *Acta Mater.*, 2010, vol.
534 58, pp. 5646–53.
- 535 32 V.V. Korolev, Y.V. Kucherinenko, A.M. Makarevich, B.B. Straumal, and P.V.
536 Protsenko: *Mater. Lett.*, DOI:10.1016/j.matlet.2017.03.076.
- 537 33 J.J. Bean and K.P. McKenna: *Acta Mater.*, 2016, vol. 110, pp. 246–57.
- 538 34 M.W. Finnis and J.E. Sinclair: *Philos. Mag. A*, 1984, vol. 50, pp. 45–55.
- 539 35 M.S. Daw and M.I. Baskes: *Phys. Rev. Lett.*, 1983, vol. 50, p. 1285.
- 540 36 G.J. Ackland, G.J. Ackland, G. Tichy, V. Vitek, and M.W. Finnis: *Philos. Mag. A*
541 *Phys. Condens. Matter, Struct. Defects Mech. Prop.*, 1987, vol. 56, pp. 735–56.
- 542 37 F. Cleri and V. Rosato: *Phys. Rev. B*, 1993, vol. 48, p. 22.
- 543 38 A.P. Sutton and J. Chen: *Philos. Mag. Lett.*, 1990, vol. 61, pp. 139–46.

- 544 39 M.S. Daw, S.M. Foiles, and M.I. Baskes: *Mater. Sci. Reports*, 1993, vol. 9, pp. 251–
545 310.
- 546 40 H. Gleiter and B. Chalmers: *High-Angle Grain Boundaries*, vol. 16, Pergamon Press
547 Oxford, 1972.
- 548 41 D. Chatain, V. Ghetta, and P. Wynblatt: *Interface Sci.*, 2004, vol. 12, pp. 7–18.
- 549 42 V.V. Korolev, Y.V. Kucherinenko, and P.V. Protsenko: *Metall. Mater. Trans. A Phys.*
550 *Metall. Mater. Sci.*, DOI:10.1007/s11661-018-4990-8.
- 551 43 N. Eustathopoulos, M.G. Nicholas, and B.B. Drevet: *Wettability at High*
552 *Temperatures*, vol. 3, 1999.
- 553 44 M. Nakamoto, M. Liukkonen, M. Friman, E. Heikinheimo, M. Hämäläinen, and L.
554 Holappa: *Metall. Mater. Trans. B Process Metall. Mater. Process. Sci.*, 2008, vol. 39,
555 pp. 570–80.
- 556 45 J. Zhao and B.L. Adams: *Acta Crystallogr. Sect. A*, 1988, vol. 44, pp. 326–36.
- 557 46 L.S. Shvindlerman and B.B. Straumal: *Acta Metall.*, 1985, vol. 33, pp. 1735–49.
- 558 47 B.W. Krakauer and D.N. Seidman: *Acta Mater.*, 1998, vol. 46, pp. 6145–61.
- 559 48 D.G. Brandon: *Acta Metall.*, 1966, vol. 14, pp. 1479–84.
- 560 49 K. Miyazawa, Y. Iwasaki, K. Ito, and Y. Ishida: *Acta Crystallogr. Sect. A*, 1996, vol.
561 A52, pp. 787–96.
- 562 50 H. Gleiter: *Acta Metall.*, 1970, vol. 18, pp. 23–30.
- 563 51 B. Straumal, Y. Kucherinenko, and B. Baretzky: *Rev. Adv. Mater. Sci.*, 2004, vol. 7,
564 pp. 23–31.
- 565 52 A. Morawiec: *Acta Mater.*, 2000, vol. 48, pp. 3525–32.

566

567

568 **Figure 1.** Optical micrograph of foil surface and 2D profile of grain boundary groove fitted with
569 quadratic polynomials to extract dihedral angles ψ (see insert).

570 **Figure 2.** The 515 experimentally determined misorientations represented in the fundamental zone
571 of Rodrigues-Frank space.

572 **Figure 3.** Grain boundary energy vs misorientation angle for the copper foil studied in this work.

573 **Figure 4.** Grain boundary energy of low angle grain boundaries of mixed type (copper foil, 1000°,
574 this study) compared with grain boundary energy of low angle $\{100\}$ tilt and twist grain boundaries
575 in copper bicrystals at 1065°^[15].

576 **Figure 5.** Grain boundaries with misorientation angle 58°–62.8° in Rodrigues-Frank space. The
577 points in the red zone correspond to $\Sigma 3$ according to the Brandon criterion ($\theta_0 = 15^\circ$).

578 **Figure 6.** Dependence of grain boundary energy and frequency of occurrence, which is normalized
579 by the frequency generated from random simulation accounting for foil texture. Full range of general
580 grain boundary energy is denoted by hatched area.

581 **Figure 7.** Correlation between the total grain boundary area (red) of each grain boundary fraction
582 and the average area of a single GB (blue) in the corresponding grain boundary energy range.

583 **Figure 8.** Grain boundary energy as a function of misorientation angle and tilt/twist relation for
584 copper foil.

585 **Figure 9.** (left) Grain boundary energy distribution as a function of grain boundary plane orientation
586 for nickel^[4] (the figure was kindly provided by Prof. G.S. Rohrer, Carnegie Mellon University) and
587 (right) copper (this work).

588 **Figure 10.** GB energy values calculated by the function developed in ref.^[8] vs those obtained from
589 the experiment with copper foil (a) and calculated by means of molecular statics in this work (b).

590 **Figure 11.** Azimuthal projection of GB plane orientation for 74 symmetrical GBs selected from the
591 experimental data set (cycles) superimposed with GBED obtained by smoothing of molecular statics
592 (MS) calculated values of GB energies for 400 symmetrical tilt GBs in copper.

593 **Figure 12.** Grain boundary energy for symmetrical GBs vs twist angle for (a) $\{111\}$, (b)
594 $\{110\}$, and (c) $\{311\}$ orientations. Deviation from the low index plane is less than 6° for all
595 the presented points.